Atmos. Chem. Phys. Discuss., 9, 21581–21618, 2009
www.atmos-chem-phys-discuss.net/9/21581/2009/

Atmospheric Chemistry and Physics Discussions

This discussion paper is/has been under review for the journal *Atmospheric Chemistry and Physics (ACP)*. Please refer to the corresponding final paper in *ACP* if available.

Validation of the GRAPE single view aerosol retrieval for ATSR-2 and insights into the long term global AOD trend

G. E. Thomas[1], C. A. Poulsen[2], R. Siddans[2], A. M. Sayer[1], E. Carboni[1], S. H. Marsh[1,*], S. M. Dean[1,], R. G. Grainger[1], and B. N. Lawrence[2]**

[1]Atmospheric, Oceanic and Planetary Physics, University of Oxford, Oxford, UK
[2]Space Science and Technology Department, Rutherford Appleton Laboratory, Didcot, Oxfordshire, UK
[*]present address: Department of Medical Physics and Bioengineering, Christchurch Hospital, New Zealand
[**]present address: National Institute of Water and Atmospheric Research, Wellington, New Zealand

Received: 24 June 2009 – Accepted: 28 September 2009 – Published: 14 October 2009

Correspondence to: G. E. Thomas (gthomas@atm.ox.ac.uk)

Published by Copernicus Publications on behalf of the European Geosciences Union.

Abstract

The Global Retrieval of ATSR Cloud Parameters and Evaluation (GRAPE) project has produced a global data-set of cloud and aerosol properties from the Along Track Scanning Radiometer-2 (ATSR-2) instrument, covering the time period 1995–2001. This paper presents the validation of aerosol optical depths (AODs) from this product against AERONET sun-photometer measurements, as well as a comparison to the Advanced Very High Resolution Radiometer (AVHRR) optical depth product produced by the Global Aerosol Climatology Project (GACP).

The GRAPE AOD over ocean is found to be in good agreement with AERONET measurements, with a correlation of 0.79 and a best-fit slope of 1.0±0.1, but with a positive bias of 0.08±0.04. Although the GRAPE and GACP datasets show reasonable agreement, there are significant differences. These discrepancies are explored, and suggest that the downward trend in AOD reported by GACP may arise from changes in sampling due to the orbital drift of the AVHRR instruments.

1 Introduction

Atmospheric aerosols play an important role in determining the Earth's radiative balance, both through their absorption and scattering of radiation (the so-called direct aerosol effect, Yu et al., 2006) and through their influence on cloud properties (indirect effects, Lohmann and Feichter, 2005). Aerosol effects remain one of the primary uncertainties in our understanding of the climate system (IPCC, 2007), so an understanding of the global aerosol distribution and its evolution over time are vital for improving our ability to characterise and predict the climate's response to anthropogenic activity.

Remote sensing of aerosol properties from imaging satellite radiometers is key in providing a global picture of the role of atmospheric aerosol. Although in situ and ground based measurements of aerosol can provide a very detailed picture of aerosol properties in a given location, satellite remote sensing is currently the only method by

ACPD

9, 21581–21618, 2009

which a truly global measure of the distribution and evolution of aerosol on a continuous and timely basis can be obtained. Although there are now many such products available (Veefkind et al., 1998; Mishchenko et al., 1999; Martonchik et al., 2002; von Hoyningen-Huene et al., 2003; Remer et al., 2005; Grey et al., 2006), most do not cover the period before 2000 and thus are currently of limited use in investigating long term changes. In addition, the limited amount of information available from passive radiometers, combined with the large number of factors which influence the top of atmosphere signal, mean that the retrieval of aerosol properties using such instruments must rely on many assumptions about both the nature of the aerosol (composition, size distribution, height distribution and mixing state, for instance) and surface/atmospheric parameters (e.g. surface BRDF, atmospheric trace-gas concentration). These assumptions reduce the accuracy of aerosol retrievals in general and mean that no one algorithm or instrument can provide accurate estimates of aerosol loading in all situations. To provide an accurate picture of global atmospheric aerosol loading and evolution there is a need for further well-characterised satellite aerosol products, particularly if they improve the aerosol record prior to the current century.

The Along Track Scanning Radiometer series of instruments[1] are ideally suited to meeting this need. These instruments can provide a nearly continuous record of aerosol properties from 1995, giving continuity to the end of the next decade with the Sea and Land Surface Temperature Radiometer (SLSTR). This paper characterises the aerosol optical depth (AOD) derived from ATSR-2 as part of the Global Retrieval of ATSR Cloud Parameters and Evaluation (GRAPE) project, which provides AOD and effective radius from 1995–2001. Descriptions of the instrument, the GRAPE product and the retrieval scheme are given in Sect. 2, while the AOD over ocean is validated against the Aerosol Robotic Network (AERONET) of sun photometers in Sect. 3. Section 4 compares the GRAPE AOD over ocean with the Global Aerosol Climatology Project (GACP) AOD product derived from the Advanced Very High Resolution Radiometer (AVHRR) instruments and provides insights in the long term trend in global

[1] Excluding the first example, ATSR-1, which lacked channels in the visible.

mean AOD evident in the GACP dataset.

2 Instrument and algorithm descriptions

2.1 ATSR-2

ATSR-2 (Mutlow et al., 1999) was successfully launched on board the second of the European Space Agency's Environment Research Satellites (ERS-2) on the 21st of April 1995. The primary object of the instrument was the continuation of the high-accuracy sea surface temperature (SST) record begun with the ATSR-1 instrument in 1990. The instrument ceased operation in 2008, but pointing difficulties due to gyro failure on the ERS-2 satellite meant that post 2001 data only became readily available in the past year. A successive similar instrument Advanced ATSR (AATSR) was launched on board Envisat in March 2002 and is expected to operate until 2012. AATSR will itself be superseded by the Sea and Land Surface Temperature Radiometer (SLSTR), which is due to be launched aboard the Sentinel-3 platform in 2014.

The ATSR-2 instrument has seven channels at 0.55, 0.67, 0.87, 1.6, 3.7, 11.0, 12.0 µm and measures a 512 km swath orthogonal to the satellite's direction of flight, with a nadir view resolution of 1×1 km. The distinguishing feature of the ATSR series of instruments is their so-called dual-view system. The instrument uses a rotating scan mirror to sample radiance in a swath centred directly below the satellite (known as the nadir view) and a second view angled at approximately 55° from vertical in the direction of the satellite's orbit (the forward view). This results in two measurements of each location, with atmospheric path lengths which differ by a factor of two. This measurement system is key (along with the more traditional 11 and 12 µm split-window method) to producing the high precision SST measurements that are the primary aim of the instruments. The dual-view system has also been widely used to separate atmospheric and surface contributions to the top of atmosphere (TOA) signal when using ATSR-2 and AATSR to retrieve aerosol and surface properties (Veefkind et al., 1998; Grey et al.,

2006; Thomas et al., 2009a).

The instrument was designed to have exceptional long term sensitivity and stability of calibration. For thermal calibration the ATSR instruments have two on-board black bodies at known temperatures. Radiation from these is measured during each scan and used to provide a continuous re-calibration of the instrument. This makes it possible to determine single channel equivalent temperatures correct to ±0.05 K. The shortwave channels of the instruments are calibrated by viewing solar radiation through an opal diffuser once an orbit. The ATSR-2 instrument has also been vicariously calibrated (Smith et al., 2002), showing that measured visible channel radiance is accurate to better than 4% and the infrared channels to better than 1 K.

2.2 GRAPE

The GRAPE project has produced a 5 year (June 1995–January 2001) climatology of aerosol and cloud properties from ATSR-2. Both cloud and aerosol properties were retrieved using the Oxford-RAL Aerosol and Cloud (ORAC) algorithm (Thomas et al., 2009b). The aerosol products produced are aerosol optical depth at 0.55 µm and effective radius. The cloud products are: cloud top temperature, pressure and height, cloud fraction, optical depth, effective radius, phase (water or ice) and liquid water path. The resolution of the data in this data set is ∼4 km. GRAPE version 3 AOD is validated in this paper.[2] Although the GRAPE project is now complete, development of the product is ongoing under the support of the NERC National Centre for Earth Observation (NCEO). This will include the processing of the post 2001 ATSR-2 data and AATSR data with the GRAPE version 3 algorithm.

[2]GRAPE was a UK Natural Environment Research Council (NERC) project. The full GRAPE data-set is available for use from the British Atmospheric Data Centre. See http://badc.nerc.ac.uk/data/grape/ for further details

ACPD
9, 21581–21618, 2009

2.3 The ORAC retrieval algorithm

The ORAC aerosol retrieval used in GRAPE is described in detail by Thomas et al. (2009b), but is summarised here for completeness. The algorithm is an optimal estimation scheme designed to allow the retrieval of aerosol from near-nadir satellite radiometers. The aerosol retrieval used in this study is a development of the Enhanced Cloud Processor developed by Watts et al. (1998). The retrieval utilises the Levenberg-Marquardt algorithm to fit modelled radiances to the satellite measurements in a combination of visible/near infrared channels.

The forward model uses TOA reflectance and atmospheric transmission look up tables (LUTs) calculated using the plane-parallel DIScrete Ordinates Radiative Transfer (DISORT) code (Stamnes et al., 1988). The LUTs account for both gas absorption (as given by MODTRAN (Berk et al., 1998) for a single reference atmosphere) and Rayleigh scattering. The GRAPE project uses a predefined geographical distribution of differing aerosol types, based on those described in the Optical Properties of Aerosols and Clouds (OPAC) database (Hess et al., 1998). The aerosol types and geographical distribution used in GRAPE are shown in Fig. 1. These types define the optical properties and a priori effective radius used in the retrieval. In order to produce LUTs which are a function of aerosol effective radius, the size distribution of the aerosol types are perturbed by varying the mixing ratios of the different components which make up each aerosol type from the values prescribed in OPAC. Mie code (Grainger et al., 2004) is then used to convert the microphysical properties (size distribution and refractive index) of the perturbed aerosol classes into optical properties. The retrieval of aerosol effective radius thus not only implies a change in the size of the aerosol particles, but in the overall composition of the aerosol type. See Thomas et al. (2009b) for a more detailed description of the implication of this methodology.

The scheme uses surface reflectances based on the MODerate resolution Imaging Spectrometer (MODIS) surface Bi-Directional Reflectance Distribution Function (BRDF) product, MOD43B, (Jin et al., 2003) over land and an ocean reflectance model

ACPD
9, 21581–21618, 2009

based on the Cox and Munk (Cox and Munk, 1954) algorithm for ocean surface reflectance with a wind correction proposed by Watts et al. (1996), driven by wind fields from European Centre for Medium-range Weather Forecasting (ECMWF) reanalysis data. As the MODIS BRDF product is only available from 2000 onwards, data for the equivalent date and location from 2002 are used to provide the surface reflectance. Errors resulting from this approximation are a major limiting factor to the accuracy of the GRAPE aerosol product over land.

The primary parameters retrieved by ORAC are aerosol optical depth at 0.55 µm and effective radius. In addition, the algorithm allows small changes in the overall surface reflectance, although the spectral shape of the surface is fixed. Due to the lack of cloud masks in the ungridded level 1 reflectance/brightness temperature data used in the GRAPE project, the scheme used two cloud flagging algorithms to classify each instrument pixel as either cloud or aerosol before the radiance data was rebinned into the 3×4 instrument-pixel bins (which provides approximately square retrieval pixels which are ~4×4 km at nadir) used in the retrieval. Over the ocean a customised scheme based on threshold tests on 11 and 12 µm brightness temperatures, spatial variability of these values and a threshold on the Normalised Vegetation Difference Index (NDVI) was used. Over the land a local implementation of the scheme described by Birks (2004) was used. Only retrieval pixels which contained no instrument pixels determined to be cloudy by these flags were used in retrieving aerosol properties.

It should be noted that the version of ORAC used to produce the GRAPE dataset made the assumption of a Lambertian surface reflectance. As a result of this assumption, it is not possible to make use of the dual-view capability of the ATSR instruments. Therefore the GRAPE aerosol product is derived from the nadir view only. Subsequent development of the ORAC algorithm has included a dual-view aerosol and surface reflectance retrieval (Thomas et al., 2009a) utilising a BRDF description of the surface reflectance, which has been applied to ATSR-2 and AATSR data as part of the GlobAEROSOL (2009) project.

The analysis undertaken by Thomas et al. (2009b) showed that, in the configuration

used in GRAPE, the ORAC retrieval has limited sensitivity to aerosol effective radius. For this reason, and because of the limited a priori knowledge of the land surface reflectance, only AOD over ocean is analysed in this paper.

3 Validation against AERONET

The primary aerosol property given by most satellite tropospheric aerosol products is the aerosol optical depth (AOD) at some visible wavelength, and it is the estimate of this quantity from GRAPE that is validated in this paper.

The AERONET is a globally distributed federation of ground based sun/sky photometers primarily designed for monitoring the column aerosol loading. The AERONET instrumentation and data analysis schemes are described by Holben et al. (1998). In this paper we compare the GRAPE AOD to AERONET Level 2, version 2 direct-sun AOD measurements. Direct-sun AOD measurements are known to have a high level of accuracy for typical atmospheric aerosol loadings, due to the weak dependence of the retrieval on assumptions about the atmospheric state, with the estimate of total error in measured AOD of <0.01 (Holben et al., 2001). AERONET also imposes standardisation of instruments, calibration, processing, quality control and distribution, which make it the primary source of calibration data for satellite based aerosol products such as GRAPE.

When comparing AOD derived from satellite measurements with those from ground-based AERONET sun photometers it is necessary to make allowances for the very different spatial and temporal sampling of the two measurement systems. AERONET provides a high temporal resolution AOD time-series for a given location, while the satellite provides a series of spatially resolved measurements of the AOD field, often separated by several days. The method used in this study to ensure a valid comparison could be made between these two different measurement system was that presented by Ichoku et al. (2002) for the validation of Moderate Resolution Imaging Spectrometer (MODIS) AOD measurements. The method can be summarised by the following steps:

- The closest "ground-pixel" of the satellite instrument (i.e. 4 km grid box) is identified.
- AOD is extracted within a region ±5 pixels from this pixel, provided they are over the sea, providing an area of similar size to that used by Ichoku et al. (2002).
- All AERONET measurements for the given ground station are extracted with time ±30 min of the satellite overpass (which given a typical aerosol transport speed of 40 km/h is consistent with the 40 km spatial distance sampled from the satellite).
- The number of valid retrievals, mean and standard deviation of AOD from each of these samples are then used in the comparison.

In addition to the sampling difference between the two datasets, there is no AERONET measurement at 0.55 µm to compare with the GRAPE AOD. This has been addressed by interpolating a 0.55 µm AERONET value using the Ångström exponent between the 0.50 and 0.87 µm AERONET measurements.

In order to minimise the risk of the inclusion of spurious measurements in the intercomparison, it is important that both datasets have adequate quality checks applied. In the case of AERONET data, only Level 2 (which has been visually inspected and quality assured) data from a list of sites determined to be representative of their surrounding areas (S. Kinne, private communication, 2006) were used. Figure 2 shows the locations of the AERONET sites found to provide matches with the GRAPE data over the ocean using these criteria. In total there are 22 stations, most of which are concentrated in North America and Europe, providing a total of 190 individual comparisons over the five year dataset.

The quality control applied to the GRAPE level 2 data are summarised in Table 1. The tests reject retrievals which have not converged or where the forward-modelled TOA radiances are in poor agreement with those observed by the satellite, and remove data which show characteristics which are known to be indicative of conditions in which the retrieval will perform poorly. In addition, AERONET station overpasses where either

the AERONET or GRAPE AOD sample standard deviation was greater than 0.1 were also rejected as a highly variable AOD field could result in strong sampling biases between the two measurements.

A scatter plot of the 190 matches between AERONET and GRAPE is given in Fig. 3. A weighted linear least-squares fit has been performed between the two datasets, taking the uncertainty (as characterised by the standard deviation of the data included in the spatio-temporal averaging described above) in both datasets into account (Press et al., 1992). This fit reveals that the GRAPE AOD data exhibit a positive bias of 0.08±0.04 as compared to AERONET, although the slope of the fit is unity to a high level of confidence. The two datasets also show a strong correlation of 0.79.

The reason for this positive bias is difficult to unambiguously determine. However, it could be a result of the fact that, by necessity, most of the GRAPE measurements included in this comparison are over coastal waters. The a priori ocean surface reflectance used in producing the GRAPE data assumes optical properties for typical deep-ocean water and a Fresnel reflection term as a function of surface wind-speed. The model does not take the effects of increased chlorophyll or gelbstoff loading. As the sediment and plankton loading of coastal waters is often substantial, it is likely that the assumed spectral shape of the surface reflectance is typically fairly poor in these areas, which would result in a bias in the retrieved AOD. In addition Thomas et al. (2009b) show that errors in the a priori absolute surface reflectance of 0.01 or more can also result in significant errors in the AOD retrieved by the GRAPE algorithm.

The other likely source of the observed offset are the aerosol optical properties assumed in the retrievals. The climatology of aerosol type used by GRAPE assigns the OPAC maritime-clean class to the majority of ocean pixels. However, since the majority of the AERONET comparisons are coastal, many of them will contain some retrievals using the aerosol type assigned to the neighbouring land mass. Investigation into how appropriate various aerosol types are for satellite retrievals is ongoing, but lies outside the scope of this paper.

Figure 3 also shows a marked increase in the scatter for AODs greater than approx-

ACPD
9, 21581–21618, 2009

imately 0.2. This could be due to both the assumed aerosol properties in the retrieval (as episodes of elevated aerosol loading will often be associated with a perturbation from the typical background composition) and increased anisotropy in the AOD field amplifying sampling errors between the two datasets.

4 Intercomparison with GACP

Although AERONET provides a ground-truth AOD measurement which allows the absolute accuracy of the GRAPE aerosol product to be assessed, it provides sparse spatial coverage, with large areas of the globe completely empty of measurements. Additionally, for the period of the GRAPE mission, the AERONET temporal coverage is generally quite sparse and does not offer much scope for time-series analysis on the data. In order to examine both the global distribution of AOD provided by GRAPE and its evolution through the five year dataset, a contemporary dataset with similar spatial and temporal coverage is required for comparison.

The Advanced Very High Resolution Radiometer (AVHRR) series of instruments are an ideal candidate to provide this comparative dataset, as they provide coverage throughout the GRAPE period and operate with similar spectral bands to ATSR-2. AVHRR measures the reflectance of the Earth in five relatively wide (in comparison with more recent satellite radiometers) spectral bands. These are centred around 0.6, 0.9, 3.7, 11 and 12 µm. The first AVHRR instrument lacked the 11 µm channel, while the latest version (AVHRR/3) adds a channel at 1.6 µm. These instruments have been flown on a number of different platforms by the US National Oceanic and Atmospheric Administration (NOAA), starting with the TIROS-N satellite in 1978. The latest versions of the instrument are carried on board the MetOp platform operated by EUMETSAT.

The AVHRR aerosol data used in this analysis are those produced by GACP (Geogdzhayev et al., 2002, 2005). GACP was a major research effort to produce a 23-year global aerosol climatology compiled from a retrieval using the first two channels, supplemented with other data sets at later dates. The data is provided on an equal angle

1×1° lat-lon grid and has been validated against ship borne radiometers (Liu et al., 2004; Smirnov et al., 2006). The time period covered by the GRAPE dataset is almost identical to that covered by the NOAA-14 AVHRR instrument in the GACP dataset.

GACP is one of two important aerosol retrievals developed for AVHRR, the second being the Pathfinder Atmosphere (PATMOS) algorithm (Stowe et al., 2002). Several variants of the PATMOS product have been developed and, although they are not included in this study, have been comprehensively compared with the GACP dataset (Zhao et al., 2008). Recently a decreasing trend in globally averaged AOD has been reported from both GACP (Mishchenko et al., 2007b) and PATMOS (Zhao et al., 2008).

In order to compare GRAPE and GACP data, the GRAPE AOD data have been composited into 1×1° monthly composites of the same form as the GACP data. This process was complicated by the fact that when one is combining large sets of data derived from an optimal estimation retrieval scheme, such as ORAC, simple averaging can produce a result that is biased towards the a priori value used in the retrieval. The result returned by an optimal estimation algorithm can be viewed as a mean of the fit to the measurements and the a priori estimate, weighted by the uncertainty in each:

$$\frac{\tau}{\sigma^2} = \frac{\tau_m}{\sigma_m^2} + \frac{\tau_a}{\sigma_a^2}, \quad (1)$$

where τ is the retrieved estimate of AOD, with uncertainty σ, τ_m and σ_m are the proportion of the retrieved value determined from the fit to the measurements, with its associated uncertainty, while τ_a and σ_a are the a priori and its uncertainty. It is clear that if a simple mean is taken from N samples of such data, where all retrievals use the same a priori (which is the case for AOD in the GRAPE retrieval), the a priori will receive N times its correct weighting in the average. Generally, this effect will be negligible because Eq. (1) will be very heavily weighted towards the measurement information, but for large ensembles of data or for relatively poorly constrained retrieval results, it can become significant. The values for τ and σ are products of the retrieval and, in the case of GRAPE, $\log_{10}(\tau_a)=-1.0\pm1.0$ (AOD is retrieved on a logarithmic

ACPD
9, 21581–21618, 2009

scale by ORAC). Note also that, by definition

$$\frac{1}{\sigma^2} = \frac{1}{\sigma_m^2} + \frac{1}{\sigma_a^2}. \quad (2)$$

Combining Eqs. (1) and (2) we can derive the value of AOD defined by the fit to the measurements alone

$$\tau_m = \frac{(\sigma\sigma_a)^2}{\sigma_a^2 - \sigma^2}\left[\frac{\tau}{\sigma^2} - \frac{\tau_a}{\sigma_a^2}\right]. \quad (3)$$

A weighted mean value for AOD, with the correct a priori weighting, can then be calculated using the expression

$$\bar{\tau} = \frac{\left[\sum \frac{\tau_m}{\sigma_m^2}\right] + \frac{\tau_a}{\sigma_a^2}}{\left[\sum \frac{1}{\sigma_m^2}\right] + \frac{1}{\sigma_a^2}}, \quad (4)$$

where the summations are over all the samples in the average.

Global maps of ATSR-2 (computed using Eq. 4) and GACP AOD are shown in Fig. 4. Both datasets show very similar patterns of AOD, with a level of agreement which compares favourably with other comparisons of satellite derived aerosol optical depth (Myhre et al., 2004, 2005; Kinne et al., 2003). There are, however, some noteworthy differences between the two datasets.

Firstly, GRAPE has some anomalously high optical depths at high latitudes. This is evidence of sea ice contamination of the GRAPE product, resulting in an a priori underestimate of surface reflectance and correspondingly poor retrievals. This is a known issue in the version 3 GRAPE product and will be corrected in later variants. It should also be noted that in the time-series analysis in Sects. 4.1 and 4.2, a point by point comparison was used, and thus did not include ice contaminated points from GRAPE (as these points are not present in the GACP data).

The GRAPE product also shows somewhat higher optical depths in many regions of continental outflow, particularly in the case of the Atlantic African biomass-burning plume and Asian plume across the Pacific. In both products such plumes are retrieved using maritime aerosol optical properties, although the precise properties assumed are not the same in each product. Thus it is possible that discrepancies in optical depth between each product, especially systematic differences revealed by long term averaging as in Fig. 4, are a result of the difference in assumed aerosol properties. This hypothesis is further supported by the fact that the GRAPE AOD shows a general trend to be slightly higher than the GACP value. However, it is not only the assumed aerosol optical properties which could explain the discrepancies between the two datasets. Other a priori assumptions, most notably cloud clearing and surface reflectance, can easily result in even larger discrepancies than assumptions about the aerosol itself. For example, the one region where the GACP AOD is systematically higher than the GRAPE estimate is in the Southern Ocean, a region characterised by very high winds and a very high percentage of cloudy days. It seems probable that this discrepancy is due to differences in cloud flagging (with GRAPE flagging heavy aerosol loading as cloud, or GACP incorrectly identifying small amounts of cloud as aerosol) or the description of the wind dependence of the surface reflectance. However, with only $1\times1^{\circ}$ monthly GACP data available, it is not possible to clearly identify the reasons behind such discrepancies.

4.1 Global time-series comparison

Global mean ocean optical depths were calculated from the $1\times1^{\circ}$ ATSR-2 and AVHRR monthly fields described above. To ensure consistency, only grid boxes containing data from both instruments were included in the calculation of the averages. The results are shown in Fig. 5. In order to investigate trends in the two datasets, a five parameter equation has been fit to the time series. The function used in the fit is given by Eq. (5) and consists of a linear trend superimposed on a sinusoid with a yearly period, with

a linear trend in amplitude:

$$y(t) = a_0 + a_1 t + (a_2 + a_3 t) \sin\left(\frac{t + a_4}{182.624}\right), \quad (5)$$

where t is time in days, and a_i are the fitted parameters. This function was chosen over a simple linear fit to the data to minimise the influence of the seasonal cycle[3] on any apparent multi-annual trend in the data. The fits using this equation are included in Fig. 5, as are the linear trend parts of the fits (i.e. $a_0 + a_1 t$).

Figure 5 shows a significant discrepancy between the two datasets, with GRAPE showing consistently higher AOD (with the difference being on the order of 0.01) and showing a positive trend, rather than the negative one consistently found in AVHRR analyses. Additionally, the GRAPE data display a distinct yearly cycle, which is not present in the GACP data. This difference and the offset in the global mean AOD will be discussed in the next section, but first the curve fitting will be described further.

The function given in Eq. (5) was fit using weighted least squares, with each point weighted by the standard error on the mean:

$$\delta\bar{\tau}_g = \frac{\sigma(\bar{\tau}_g)}{\sqrt{n}}, \quad (6)$$

where $\bar{\tau}_g$ is the global mean value of AOD for a given month, calculated from n samples, and $\sigma(\bar{\tau}_g)$ is the associated standard deviation. One can propagate this error into an estimate of an error in each of the parameters in Eq. (5) using the gradient of this function with respect to that parameter:

$$\frac{1}{\delta a_i^2} = \sum_{j=1}^{N} \left(\frac{\partial y}{\partial a_i}\right)^2 \frac{1}{\delta\bar{\tau}_{g,j}^2} \quad (7)$$

where the right hand side is summed over the N monthly global mean values in the time-series. However, this will produce an error estimate based on the assumption that

[3]Which is especially strong in some regions, see Sect. 4.2

the model fit to the data describes all the systematic variability in the model (i.e. that any differences between the data and fitted function are due solely to the random variability in the data described by the $\sigma(\bar{\tau}_g)$ values). Since it is highly unlikely that the variability in the global mean AOD can be completely described by Eq. (5), these error estimates will clearly be an underestimate of the true uncertainly in the fitted parameters.

We address this problem by scaling the δa_i values by the χ^2 statistic for the fit, where χ^2 is defined as

$$\chi^2 = \sum_j \left(\frac{y_j - \bar{\tau}_{g,j}}{\sigma(\bar{\tau}_{g,j})} \right)^2, \quad (8)$$

where y_j are the fitted values of Eq. (5) for each monthly average $\bar{\tau}_{g,j}$. In the case where y_j and $\bar{\tau}_{g,j}$ are samples from the same distribution with standard deviation $\sigma(\bar{\tau}_{g,j})$, χ^2 has the expectation value $N-M$, where $M=5$ is the number of parameters in Eq. (5) and N is as defined above (i.e. the number of degrees of freedom for the fit). Thus, by rescaling the uncertainties on the parameters by

$$\delta a_i' = \sqrt{\frac{\chi^2}{N-M}} \delta a_i, \quad (9)$$

we are effectively forcing the uncertainties in a_i to reflect the true discrepancy between the data and model fit.

Following this procedure, we find that the linear component of the fit to the GRAPE data (the black dotted line in Fig. 5) is $\bar{\tau}_g(t)=(0.142\pm0.002)+(6.5\pm2.0)\times10^{-6}t$, where $t=0$ is defined to correspond to 1 June 1995, corresponding to the first point in the time-series. Similarly, the fit to GACP data is $\bar{\tau}_g(t)=(0.135\pm0.003)-(5.0\pm2.4)\times10^{-6}t$. It is worth noting that the decadal trend seen in the GACP data over the GRAPE data period (0.018 ± 0.009 decade^{-1}) is very close to that found by Mishchenko et al. (2007b) for the entire post Pinatubo eruption dataset. However, due to the relatively short time-span of GRAPE the trends in both datasets are not significant at the 99% confidence, as was case for the trend found by Mishchenko et al.

4.2 Regional time-series comparison

The discrepancies between the two time-series in Fig. 5 can largely be attributed to regional differences between the two dataset. To investigate regional trends and differences between the two datasets, the ocean regions defined by Quaas et al. (2008) have been used. These regions are shown in Fig. 6 and the time-series for GACP and GRAPE data within these regions are given in Fig. 7. Equation (5) has again been fitted to the time-series to reveal long term trends in the data and the gradient of the trend line for each region is listed in Table 2.

Figure 7 reveals a complicated picture behind the differences seen in the global comparison; the level of agreement between the two datasets is clearly different for different regions:

- Both northern regions show a large discrepancy in the seasonal cycles between the two datasets, with GRAPE showing a much stronger cycle than is present in GACP. In both cases there is reasonable agreement between the two time-series during the low-AOD section of the GRAPE cycle, but then the GACP values drop away, while GRAPE continues to increase. It is interesting to note that GACP does show a strong seasonal cycle in the NPO, but it is approximately 3 months out of phase. The NPO is also notable in that the GRAPE data show an increasing trend (due to an increasing amplitude of the season cycle while the lower limit of the cycle remains approximately constant).

- The tropical oceans show little evidence of a season cycle, except for the TAO (which shows evidence of the cycle of African biomass burning). With the exception of the TIO, the two datasets show better overall agreement than in the northern oceans. It is also worth noting that the two most statistically significant increasing trends seen in the GRAPE data occur in the TIO and TPO.

- Overall, the southern oceans show the best agreement between the two datasets. Both show a seasonal cycle of similar magnitude and phase and have similar

mean values. However, GACP shows a negative trend in all three regions, but this is not present in the GRAPE data.

Perhaps the most surprising difference between the GACP and GRAPE time-series is the negative trend seen in the GACP southern ocean results. The presence of a decreasing trend in AOD in the Southern oceans is a surprising result since the aerosol burden in these regions is primarily generated by wind driven spray and phytoplankton-generated dimethyl sulphide from the ocean surface.

Time-series of daily mean 10 m altitude wind speed from European Centre for Medium Range Weather Forecasting (ECMWF) reanalysis data and monthly mean chlorophyll-*a* concentration from the GlobCOLOUR dataset (Pinnock et al., 2007) are shown in Fig. 8. The wind speed shows a slight increasing trend of $0.028 \pm 0.005\,\mathrm{ms}^{-1}\,\mathrm{decade}^{-1}$, but this only amounts to a 0.2% change in the average wind speed over the 5 years. Although GlobCOLOUR data only becomes available towards the end of 1997 (with the launch of the SeaWIFS instrument), there is no significant trend apparent in the data ($-0.01 \pm 0.04\,\mathrm{mg\,m}^{-3}\,\mathrm{decade}^{-1}$). Thus, it seems unlikely that the AOD trend found in GACP data can be attributed to changes in the wind speed or ocean ecosystem.

At high latitudes satellite radiometers are susceptible to temporal sampling biases. In the winter months, the high-latitude limits of the northern and southern regions will be truncated by the solar zenith angle limits of the retrievals. This will introduce a cyclical sampling bias into both datasets, which could result in an spurious seasonal cycle in the mean AOD. Figure 9 shows the latitude limits of both datasets throughout the period of comparison. In the case of the GRAPE dataset, the actual limit lies equatorward of the defined 60° limit for November–January in the Northern Hemisphere and for May–July in the Southern Hemisphere, with a maximum discrepancy of 12°.

Due to the changes in AVHRR overpass times, the GACP dataset shows a more complicated story, with an increase in both the size of the truncation of the the high latitude limits of the northern and southern regions, and in the number of months a year so effected, as the lifetime of each individual AVHRR instrument progresses.

ACPD
9, 21581–21618, 2009

Geogdzhayev et al. (2005) investigated the effect of this orbital drift on the GACP global mean AOD, from the perspective of the total number of samples included in the mean, and the effect of the seasonal cycle on the maximum/minimum latitudes on hemispheric mean AOD. However, an analysis of the effects of the drift on this seasonal cycle was not presented.

Given the band of elevated AOD observed at around 60° S in the GACP results, a decreased sampling of the lower boundary of the southern ocean regions can explain the negative AOD trend observed in these regions during the period covered by the GRAPE data. This also explains why no such trend is observed in the GRAPE results. It is, however, not possible to disentangle the source of the AOD seasonal cycle seen in the southern regions from the seasonal cycles of the aerosol sources shown in Fig. 8 from the cycle in the sampling seen in Fig. 9, especially as the chlorophyll-*a* concentration is derived from satellite measurements that are probably also affected by such sampling biases.

The much larger seasonal variation exhibited by the GRAPE data in the northern regions, as well as their discrepancy with the GACP results also warrants further investigation. Although northern regions are also affected by the seasonal sampling biases, it is reasonable to expect a true a cycle in aerosol loading, because of seasonal changes in both the source strength of the particles, efficiency of long-range transport and aerosol removal processes such as precipitation. Figure 10 shows time-series of monthly mean AOD from AERONET stations which lie along the western edges of the North Atlantic and Pacific Oceans. Although not temporally or spatially coincident with the majority of GRAPE time-series, this cycle is in phase with that seen in the GRAPE data, suggesting that the cycle seen by GRAPE is real. The authors can only speculate about the reasons for the discrepancy in the GACP seasonal cycle, but it is possible that the GACP analysis has flagged heavy aerosol loading events as cloud, or that the retrieval fails in such conditions. This could also explain the large positive bias GRAPE shows against GACP in the TIO region.

It is important to emphasise that the analysis undertaken in this section does not pro-

vide a validation of the absolute AODs retrieved by GRAPE. Only comparison against a ground truth measurement, such as that undertaken in Sect. 3, can provide such a validation. Some of the features seen in the GRAPE data, such as the very high values of AOD seen in the North Atlantic during the summer (Fig. 4), require further analysis and comparison with more measurements. However, this analysis has provided valuable insights into and improved confidence in the large-scale variability seen in the GRAPE data.

5 Conclusions

The GRAPE AOD product has been compared against measurements from the AERONET and the GACP AVHRR derived AOD climatology over the ocean. The GRAPE and AERONET AOD measurements show a good correlation of 0.79. A linear fit between the two data-sets produces a slope of 1.0±0.1, however the fit shows GRAPE AODs have a positive bias of 0.08±0.04. At higher AODs ($\gtrsim$0.2) the comparison also shows a much greater degree of scatter, although this could be due to sampling differences between the two measurement systems.

Comparisons between monthly mean ocean AODs between the GRAPE and GACP datasets show reasonable overall agreement between the two datasets, but there are some noticeable discrepancies. The GRAPE dataset displays some anomalously high AODs at high latitudes, which can be attributed to contamination by surface ice: a known problem with the GRAPE dataset. The GRAPE data also show noticeably higher AOD in regions affected by transportation of heavy aerosol loading from the continents. Conversely, the band of elevated AOD seen in the southern oceans in the GACP data is not apparent in the GRAPE data.

Time-series analysis of the GRAPE and GACP monthly means revealed significant differences. Globally, the GRAPE dataset shows a slightly increasing trend in AOD, as opposed to the decreasing trend which has been the headline finding of the GACP dataset (Mishchenko et al., 2007b). A regional time-series analysis showed the origins

of this disagreement. The GRAPE dataset shows stronger seasonal variation than is present in the GACP data, particularly in northern oceans (NAO and NPO), and also showed significantly higher average AODs in regions affected by continental outflow (the NAO, NPO and TIO in particular). The presence of a strong seasonal cycle in AERONET AODs in the northern ocean regions, which are approximately in phase with that seen in the GRAPE data, suggests that a higher proportion of high AOD events are not included in the GACP dataset. This could be due to either over-zealous cloud flagging or the failure of the algorithm at high AOD.

The increasing trend in global AOD seen in the GRAPE data can be attributed to increasing AOD in the NPO, TPO and TIO. All of these regions are subject to aerosol transport from regions which have undergone large scale industrialisation over the past few decades. An increasing trend in aerosol loading is not, therefore, an unexpected result. Conversely, the decreasing trend seen in the GACP data can mostly be attributed to decreasing AOD in the southern ocean regions (SAO, SPO and SIO). This is a surprising result, as the AOD in these regions is dominated by wind-generated maritime aerosol. An examination of the latitudinal limits of the two datasets reveals that the decreasing maximum latitude sampled by the AVHRR instrument in winter during the period of comparison could be a possible explanation of this trend.

Overall the GRAPE AOD over ocean dataset has been shown to have a good level of accuracy compared to AERONET AODs. The potential value of the dataset has been shown by the light this analysis has shed on the long term global aerosol trend suggested by AOD climatologies based on AVHRR measurements.

Due to the limited time period covered by the GRAPE dataset, this analysis cannot be used to draw firm conclusions about long term trends in global and regional AOD. However, the authors believe it amply displays the need for further long-term aerosol datasets. The GlobAEROSOL (GlobAEROSOL, 2009) dataset, and the ATSR-2/AATSR dataset produced by Grey et al. (2006) will both provide global AODs covering the range 1995–2007. In addition, the extension of the GRAPE dataset to include all ATSR-2 and AATSR data up to 2009 will become available in 2010.

Acknowledgements. This work was supported by the Natural Environment Research Council (grant numbers NER/T/S/2001/002, NE/B503933/1 and NE/E011187/1). Additional support was provided by the ESA Data User Element project Globaerosol.
We also greatfully acknowledge the principal investigators of the AERONET sites utilised by this work, as well as NASA Goddard for making AERONET and GACP data available.

References

Berk, A., Bernstein, L. S., Anderson, G. P., Acharya, P. K., Robertson, D. C., Chetwynd, J. H., and Adler-Golden, S. M.: MODTRAN cloud and multiple scattering upgrades with application to AVIRIS, Remote Sens. Environ., 65, 367–375, 1998. 21586

Birks A.: Improvements to the AATSR IPF relating to land surface temperature, European Space Agency Technical Note, 2004. 21587

Cox, C. and Munk, W.: Statistics of the sea surface derived from Sun glitter, J. Mar. Res., 13, 198–227, 1954. 21587

Delderfield, J., Llewellyn-Jones, D. T., Bernard, R., de Javel, Y., Williamson, E. J., Mason, I., Pick, D. R., and Barton, I. J.: The Along Track Scanning Radiometer (ATSR) for ERS-1, Proc. SPIE, 589, 114–120, 1986.

Geogdzhayev, I. V., Mishchenko, M. I., Rossow, W. B., Cairns, B., and Lacis, A. A.: Global two-channel AVHRR retrievals of aerosol properties over the ocean for the period of NOAA-9 observations and preliminary retrievals using NOAA-7 and NOAA-11 data, J. Atmos. Sci., 59, 262–278, 2002. 21591

Geogdzhayev, I. V., Mishchenko, M. I., Liu, L., and Remer, L.: Global two-channel AVHRR aerosol climatology: Effects of stratospheric aerosols and preliminary comparisons with MODIS and MISR retrievals, J. Quant. Spectrosc. Radiat. Transfer, 88, 47–59, 2004.

Geogdzhayev, I. V., Mishchenko, M. I., Terez, E. I., Terez, G. A., and Gushchin, G. K.: Regional advanced very high resolution radiometer-derived climatology of aerosol optical thickness and size, J. Geophys. Res.-Atmos., 110, D23205, doi:10.1029/2005JD006170, 2005. 21591, 21599

GlobAEROSOL: http://www.globaerosol.info, access: 28 May 2009. 21587, 21601

Grainger, R. G., Lucas, J., Thomas, G. E., and Ewen, G. B. L.: Calculation of Mie derivatives, Appl. Opt., 43, 5386–5393, 2004. 21586

Grey, W. M. F., North, P., and Los, S.: Computationally efficient method for retrieving aerosol optical depth from ATSR-2 and AATSR data, Appl. Opt., 45, 2786–2795, 2006. 21583, 21584, 21601

Hess, M., Koepke, P., and Schult, I.: Optical properties of aerosols and clouds: The software package OPAC, Bull. A. Met. Soc., 79, 831–844, 1998. 21586

Holben, B. N., Eck, T. F., Slutsker, I., Tanre, D., Buis, J. P., Setzer A., Vermote, E., Reagan, J. A., Kaufman, Y., Nakajima, T., Lavenu, F., Jankowiak, I., and Smirnov, A.: AERONET – A federated instrument network and data archive for aerosol characterization, Rem. Sens. Environ., 66, 1–16, 1998. 21588

Holben, B. N., Tanre, D., Smirnov, A., Eck, T. F., Slutsker, I., Abuhassan, N., Newcomb W. W., Schafer J. S., Chatenet B., Lavenu F., Kaufman Y. J., Castle J. V., Setzer A., Markham B., Clark D., Frouin R., Halthore R., Karneli A., O'Neill, N. T., Pietras, C., Pinker, R. T., Voss, K., and Zibordi, G.: An emerging ground-based aerosol climatology: Aerosol optical depth from AERONET, J. Geophys. Res.-Atmos., 106, 12 067–12 097, 2001. 21588

von Hoyningen-Huene, W., Freitag, M., and Burrows, J. B.: Retrieval of aerosol optical thickness over land surfaces from top-of-atmosphere radiance, J. Geophys. Res.-Atmos., 108, 4260, doi:10.1029/2001JD002018, 2003. 21583

Ichoku, C., Chu, D. A., Mattoo, S., Kaufman, Y. J., Remer, L. A., Tanre, D., Slutsker, I., and Holben, B. N.: A spatio-temporal approach for global validation and analysis of MODIS aerosol products, Geophys. Res. Lett., 29, 8006, doi:10.1029/2001GL013206, 2002. 21588, 21589

IPCC (Solomon, S., Qin D., Manning M., Chen Z., Marquis M., Averyt K. B., Tignor M., and Miller H. L. (eds.)): Climate Change 2007: The physical science basis. Contribution of Working Group I to the Fourth Assessment Report of the Intergovernmental Panel on Climate Change, Cambridge University Press, Cambridge, New York, 2007. 21582

Jin, Y., Schaaf, C. B., Woodcock, C. E., Gao, F., Li, X., Strahler, A. H., Lucht, W., and Liang, S.: Consistency of MODIS surface BRDF/Albedo retrievals: 1. Algorithm performance, J. Geophys. Res.-Atmos., 108, 4158, doi:10.1029/2002JD002803, 2003. 21586

Kinne, S., Lohmann, U., Feichter, J., Schulz, M., Timmreck, C., Ghan, S., Easter, R., Chin, M., Ginoux, P., Takemura, T., Tegen, I., Koch, D., Herzog, M., Penner, J., Pitari, G., Holben, B., Eck, T., Smirnov, A., Dubovik, O., Slutsker, I., Tanre, D., Torres, O., Mishchenko, M., Geogdzhayev, I., Chu, D. A., and Kaufman, Y.: Monthly averages of aerosol properties: A global comparison among models, satellite data, and AERONET ground data, J. Geophys. Res.-Atmos., 108, 4634, doi:10.1029/2001JD001253, 2003. 21593

Liu, L., Mishchenko, M. I., Geogdzhayev, I., Smirnov, A. Sakerin, S. M., Kabanov, D. M., and Ershov, O. A.: Global validation of two-channel AVHRR aerosol optical thickness retrievals over the oceans. J. Quant. Spectrosc. Radiat. Transfer, 88, 97–109, 2004. 21592

Lohmann, U. and Feichter, J.: Global indirect aerosol effects: a review, Atmos. Chem. Phys., 5, 715–737, 2005, http://www.atmos-chem-phys.net/5/715/2005/. 21582

Martonchik, J. V., Diner, D. J., Crean, K. A., and Bull, M. A.: Regional aerosol retrieval results from MISR, IEEE Trans. Geosci. Rem. Sens., 40, 1520–1531, 2002. 21583

Mishchenko, M. I., Geogdzhaev, I. V., Cairns, B., Rossow, W. B., and Lacis, A. A.: Aerosol retrievals over the ocean by use of channels 1 and 2 AVHRR data: sensitivity analysis and preliminary results, Appl. Opt., 38, 7325–7341, 1999. 21583

Mishchenko, M. I. and Geogdzhaev, I. V.: Satellite remote sensing reveals regional tropospheric aerosol trends, Opt. Express 15, 7423–7438, 2007.

Mishchenko, M. I., Geogdzhaev, I. V. Rossow, W. B., Cairns, B., Carlson, B. E., Lacis, A. A., Liu, L., and Travis, L. D.: Long-term satellite record reveals likely recent aerosol trend, Science, 315, 1543, doi:10.1126/science.1136709, 2007. 21592, 21596, 21600

Mutlow, C. T., Murray, M. J., Bailey, P., Birks, A. R., and Smith, D. L.: ATSR-1/2 user guide issue 1, ESA User Guide, 1999. 21584

Myhre, G., Stordal, F., Johnsrud, M., Ignatov, A., Mishchenko, M. I., Geogdzhayev, I. V., Tanré, D., Deuzé, J.-L., Goloub, P., Nakajima, T., Higurashi, A., Torres, O., and Holben, B. N.: Intercomparison of Satellite Retrieved Aerosol Optical Depth over the Ocean, J. Atmos. Sci., 61, 499–513, 2004. 21593

Myhre, G., Stordal, F., Johnsrud, M., Diner, D. J., Geogdzhayev, I. V., Haywood, J. M., Holben, B. N., Holzer-Popp, T., Ignatov, A., Kahn, R. A., Kaufman, Y. J., Loeb, N., Martonchik, J. V., Mishchenko, M. I., Nalli, N. R., Remer, L. A., Schroedter-Homscheidt, M., Tanré, D., Torres, O., and Wang, M.: Intercomparison of satellite retrieved aerosol optical depth over ocean during the period September 1997 to December 2000, Atmos. Chem. Phys., 5, 1697–1719, 2005, http://www.atmos-chem-phys.net/5/1697/2005/. 21593

Pinnock, S., D'Andon, O. F., and Lavender, S.: GlobColour – A precursor to the GMES marine core service ocean colour Thematic Assembly Centre, ESA Bulletin, European, Space Agency, 132, 42–49, 2007. 21598

Press, W. H., Teukolsky, S. A., Vettering, W. A., and Flannery, B. P.: Numerical Recipes in

Fortran 77, 2nd edn., Cambridge Univ. Press, UK, 1992. 21590
Quaas, J., Boucher, O., Bellouin, N., and Kinne, S.: Satellite-based estimate of the direct and indirect aerosol climate forcing, J. Geophys. Res.-Atmos., 113, D05204, doi:10.1029/2007JD008962, 2008. 21597
Remer, L. A., Kaufman, Y. J., Tanre, D., Mattoo, S., Chu, D. A., Martins, J. V., Li, R. R., Ichoku, C., Levy, R. C., Kleidman, R. G., Eck, T. F., Vermote, E., and Holben B. N.: The MODIS aerosol algorithm, products, and validation, J. Atmos. Sci., 62, 947–973, 2005. 21583
Rodgers, C. D.: Inverse Methods for Atmospheric Sounding: Theory and Practice, World Scientific, Singapore, 2000. 21607
Smirnov, A., Holben, B. N., Sakerin, S. M., Kabanov, D. M., Slutsker, I., Chin, M., Diehl, T, L., Remer, A., Kahn, R., Ignatov, A., Liu, L., Mishchenko, M., Eck, T. F., Kucsera, T. L., Giles, D., and Kopelevich, O. V.: Ship-based aerosol optical depth measurements in the Atlantic Ocean: Comparison with satellite retrievals and GOCART model, Geophys. Res. Lett., 33, L14817, doi:10.1029/2006GL026051, 2006. 21592
Smith, D. L., Mutlow, C.T., and Rao, C. R. N.: Calibration Monitoring of the Visible and Near-Infrared Channels of Along-Track Scanning Radiometer-2 (ATSR-2) using Stable Terrestrial Sites, Appl. Opt., 41, 515–523, 2002. 21585
Stamnes, K. Tsay, S. C., Wiscombe, W., and Jayaweera, K.: Numerically stable algorithm for discrete ordinate method radiative transfer in multiple scattering and emitting layered media, Appl. Opt., 27, 2502–2509, 1988. 21586
Stowe, L. L., Jacobowitz, H., Ohring, G., Knapp, K. R., and Nalli, N. R.: The advanced very high resolution radiometer (AVHRR) pathfinder atmosphere (PATMOS) climate dataset: Initial analysis and evaluations, J. Clim., 15, 1243–1260, 2002. 21592
Thomas, G. E., Carboni, E., Sayer, A. M., Poulsen, C. A., Siddans, R., and Grainger, R. G.: Oxford-RAL Aerosol and Cloud (ORAC): Aerosol Retrievals from Satellite Radiometers, in: Aerosol Remote Sensing Over Land, edited by: Kokhanovsky, A. A. and de Leeuw, G., Springer, Berlin, 2009. 21585, 21587
Thomas, G. E., Poulsen, C. A., Sayer, A. M., Marsh, S. H., Dean, S. M., Carboni, E., Siddans, R., Grainger, R. G., and Lawrence, B. N.: The GRAPE aerosol retrieval algorithm, Atmos. Meas. Tech. Discuss. 2, 1–46, 2009. 21585, 21586, 21587, 21590, 21607
Veefkind, J. P., de Leeuw, G., and Durkee, P. A.: Retrieval of aerosol optical depth over land using two-angle view satellite radiometry during TARFOX, Geophys. Res. Lett., 25, 3135–

3138, 1998. 21583, 21584
Watts, P. D., Allen, M. R., and Nightingale, T. J.: Wind speed effects on sea surface emission and reflection for the Along Track Scanning Radiometer, J. Atmos. Oceanic Technol., 13, 126–141, 1996. 21587
Watts, P. D., Mutlow, C. T., Baran, A. J., and Zavody, A. M.: Study on cloud properties derived from Meteosat Second Generation observations, EUMETSAT ITT no. 97/181, 1998. 21586
Yu, H., Kaufman, Y. J., Chin, M., Feingold, G., Remer, L. A., Anderson, T. L., Balkanski, Y., Bellouin, N., Boucher, O., Christopher, S., DeCola, P., Kahn, R., Koch, D., Loeb, N., Reddy, M. S., Schulz, M., Takemura, T., and Zhou, M: A review of measurement-based assessments of the aerosol direct radiative effect and forcing, Atmos. Chem. Phys., 6, 613–666, 2006, http://www.atmos-chem-phys.net/6/613/2006/. 21582
Zhao, T. X.-P., Laszlo, I., Guo, W., Heidinger, A., Cao, C., Jelenak, A., Tarpley, D., and Sullivan, J.: Study of long-term trend in aerosol optical thickness observed from operational AVHRR satellite instrument, J. Geophys. Res.-Atmos., 113, D07201, doi:10.1029/2007JD009061, 2008. 21592

Table 1. Quality control applied to GRAPE level 2 aerosol data.

Value	Criteria	Description
Iterations	>1	The retrieval must have converged and not returned the a priori state after one iteration.
Cost	<10	Retrieval must be consistent with both measurements and a priori constraints (see Rodgers (2000) or Thomas et al. (2009b) for a definition of this quantity).
550 nm surface reflectance	<0.1	A high retrieved surface reflectance is indicative of sun-glint contamination.
Effective radius	<5 µm	A very large retrieved effective radius is indicative of cloud contamination.

ACPD
9, 21581–21618, 2009

Table 2. Trends in 550 nm AOD, in units of decade^{-1}, from regional time-series. The uncertainties are the 1σ estimates propagated from the standard deviation of each point in the time-series.

Region	GRAPE		GACP	
	Mean AOD	Trend	Mean AOD	Trend
Global	0.151	0.024±0.007	0.130	–0.018±0.009
NAO	0.175	0.00±0.02	0.132	–0.03±0.01
NPO	0.169	0.04±0.02	0.131	–0.01±0.01
TAO	0.203	0.00±0.03	0.187	0.03±0.03
TPO	0.124	0.035±0.003	0.111	–0.01±0.01
TIO	0.173	0.05±0.01	0.133	0.03±0.02
SAO	0.120	0.01±0.01	0.107	–0.06±0.02
SPO	0.112	0.02±0.01	0.112	–0.07±0.02
SIO	0.129	0.02±0.01	0.120	–0.09±0.02

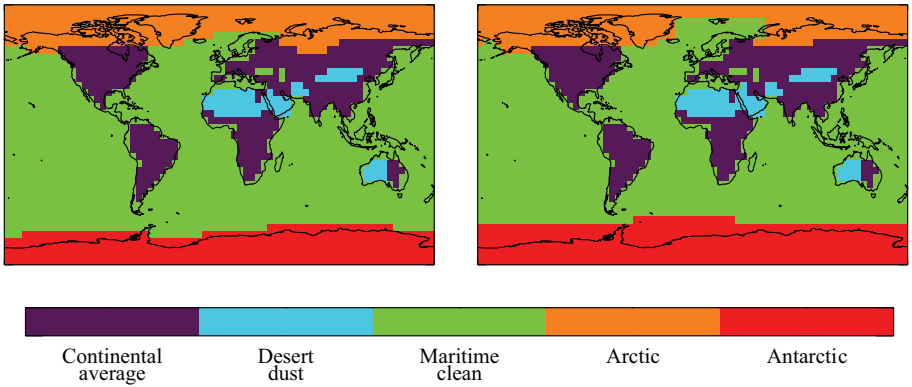

Fig. 1. The spatial distribution of aerosol types used by GRAPE. The left map shows the distribution used for Southern Hemisphere summer (October–March), the Northern Hemisphere summer (April–September) is given on the right.

ACPD
9, 21581–21618, 2009

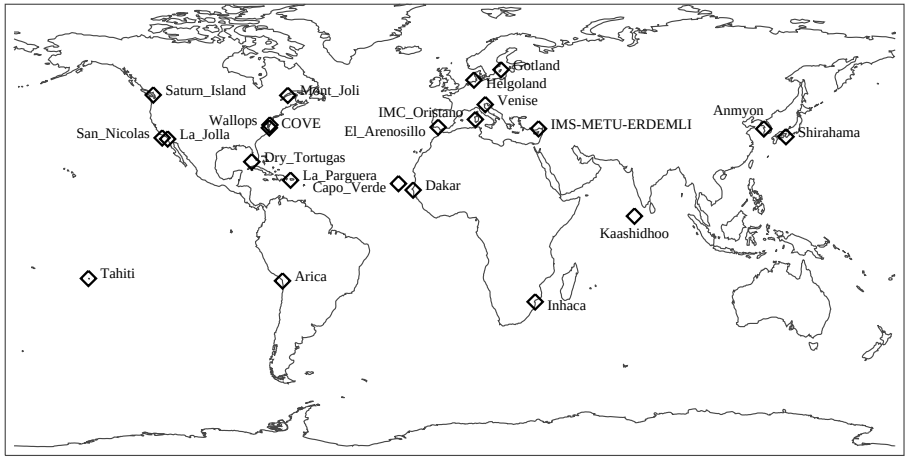

Fig. 2. Location of AERONET sites used for validation.

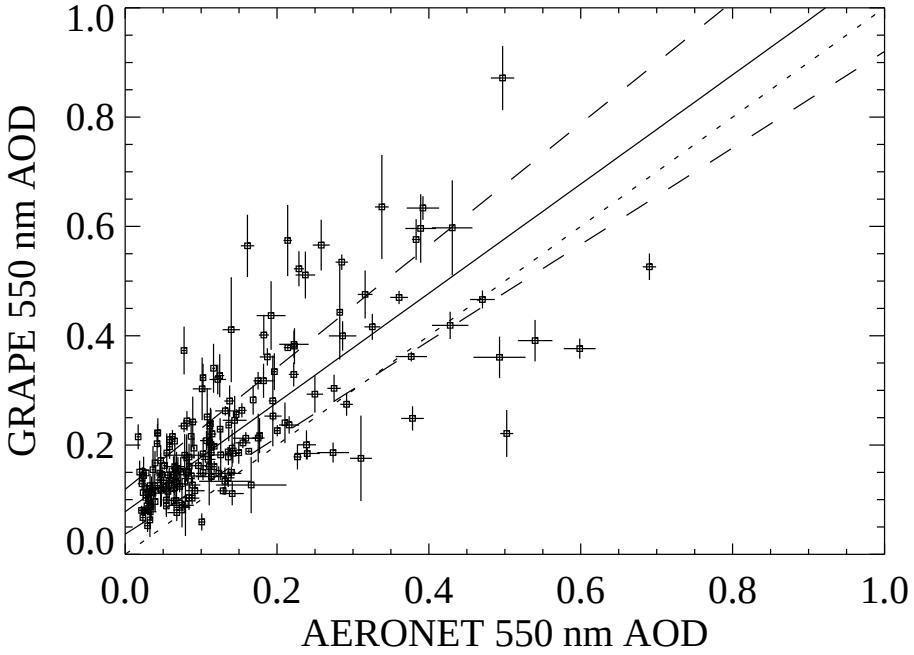

Fig. 3. AERONET comparison of ATSR-2 with the sites shown in Fig. 2. The two datasets have a correlation of 0.79 with an RMS difference of 0.13. The best-fit line (solid line, 1σ uncertainty given by dashed line) is given by the Eq. $\tau_G=(0.08\pm0.04)+(1.0\pm0.1)\tau_A$. The one-to-one line (dotted) is also included for reference.

ACPD
9, 21581–21618, 2009

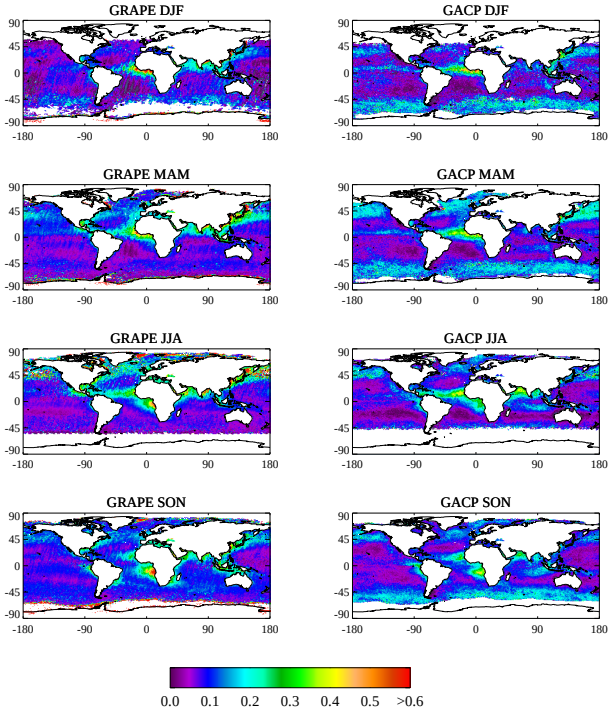

Fig. 4. Global seasonal maps of GRAPE and GACP AOD. Each plot shows the average of all monthly data, where both datasets are available. The seasons are defined as December-January-February (DJF), March-April-May (MAM) June-July-August (JJA) and September-October-November (SON).

ACPD
9, 21581–21618, 2009

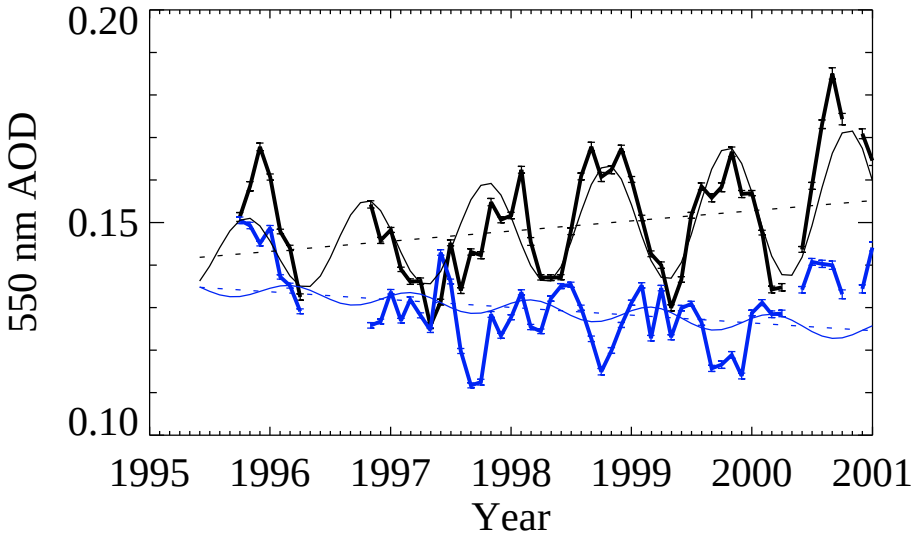

Fig. 5. Global time-series showing the comparison of AVHRR AOD with ATSR-2 AOD between 1995 and 2001. ATSR-2 data are shown in black and AVHRR in blue. The thick lines show the mean value for each month, with error bars indicating the standard error on the mean. Fits to the time-series using Eq. (5) are given by the thin solid lines, and the linear component of these fits are shown by the dotted lines.

ACPD
9, 21581–21618, 2009

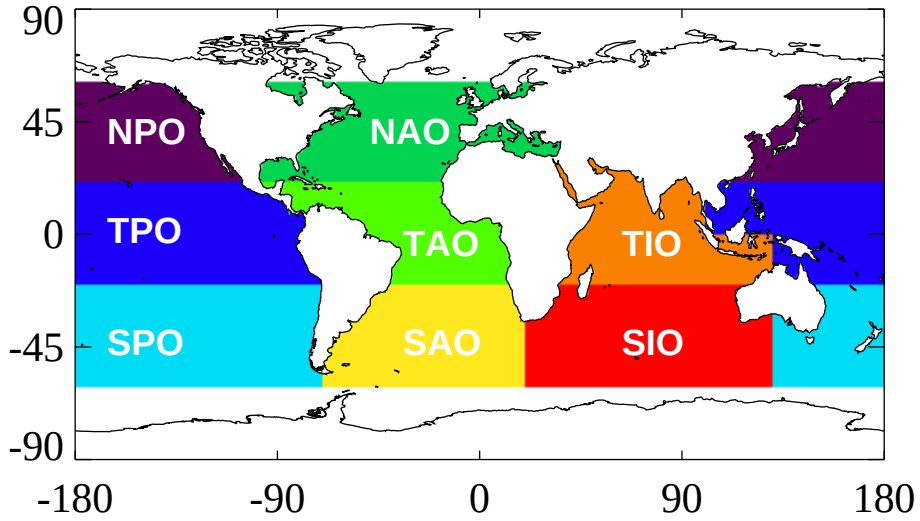

Fig. 6. The extent of the regions used in the time-series analysis. The regions are defined as follows:

NAO	North Atlantic Ocean	TAO	Tropical Atlantic Ocean
SAO	South Atlantic Ocean	NPO	North Pacific Ocean
TPO	Tropical Pacific Ocean	SAO	South Pacific Ocean
TIO	Tropical Indian Ocean	SIO	South Indian Ocean

ACPD
9, 21581–21618, 2009

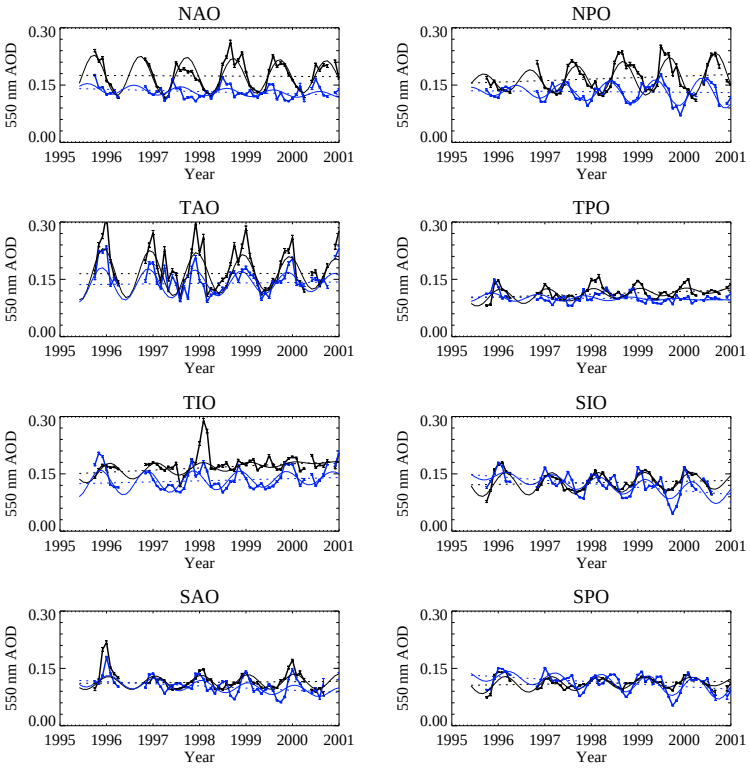

Fig. 7. Regional times series comparison of GRAPE and GACP AOD. Monthly averaged data are given by the thick-solid lines, with GRAPE in black and GACP in blue. Fits to the time-series using Eq. (5) are given by the thin solid lines, and the linear component of these fits are shown by the dotted lines.

ACPD
9, 21581–21618, 2009

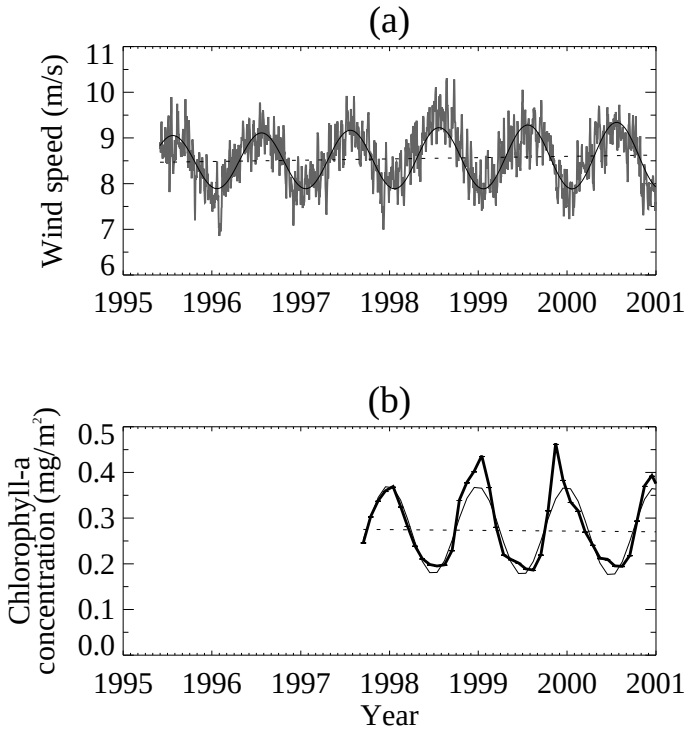

Fig. 8. Time-series of daily mean 10 m wind speed from ECMWF reanalysis **(a)** and monthly mean chlorophyll- a concentration from GlobCOLOUR **(b)** for the southern-most regions defined in Fig. 6 (SPO, SAO and SIO). Fits to the time-series using Eq. (5) are given by the thin solid lines, and the linear component of these fits are shown by the dotted lines.

ACPD
9, 21581–21618, 2009

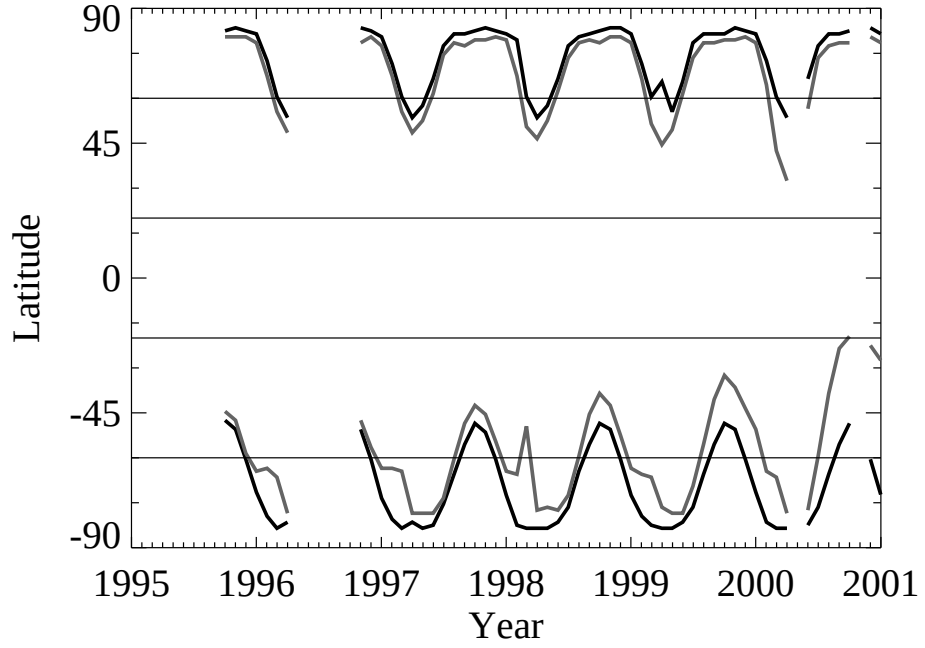

Fig. 9. Time-series of the maximum and minimum latitudes included in the GRAPE (black line) and GACP (grey line) datasets for the period covered by the GRAPE dataset. The thin horizontal lines indicate the north-south boundaries of the regions defined in Fig. 6 at ±20° and ±60°.

ACPD
9, 21581–21618, 2009

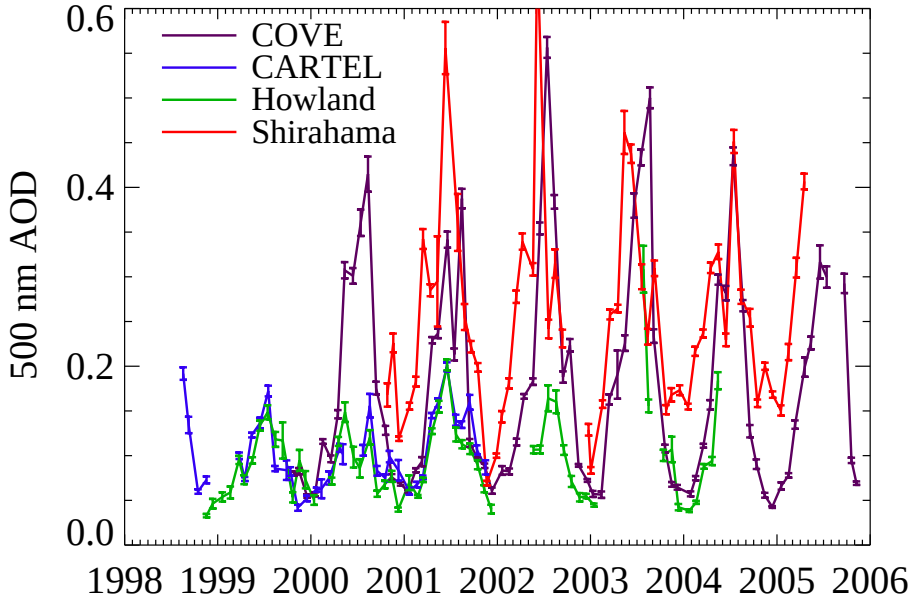

Fig. 10. Time-series of AOD from four AERONET sites along the eastern seaboards of North America (COVE, CARTEL and Howland) and Northern Asia (Shirahama).

ACPD
9, 21581–21618, 2009